Experimental Investigation and Model Development for Thermal Conductivity of α-Al_2O_3-Glycerol Nanofluids

M. Sharifpur[1]*, N. Tshimanga[1], J. P. Meyer[1] and O. Manca[2]

[1] Nanofluids Research Laboratory, Department of Mechanical and Aeronautical Engineering
University of Pretoria, Private Box 0002, Pretoria, South Africa

[2] Department of Industrial and Information Engineering,
Università degli Studi della Campania "Luigi Vanvitelli", via Roma 29, 81031 Aversa, Italy

Abstract

In order to investigate the effect of nanoparticle volume fraction, nanoparticle size and temperature on the thermal conductivity of glycerol based alumina (α-Al_2O_3) nanofluids, a set of experiments were carried out for temperature ranging from 20 ˚C to 45 ˚C. The nanofluids contained α-Al_2O_3 nanoparticles of three different sizes (31 nm, 55 nm and 134 nm) were prepared by two-step method at volume fractions ranging from 0.5% to 4%. The experimental results show that α-Al_2O_3-glycerol nanofluids have substantially higher thermal conductivity than the base fluid and the maximum enhancement of the relative thermal conductivity was 19.5% for the case of 31 nm at 4% volume fraction. The data analyses indicated that the volume fraction and size of the nanoparticles have significant effects on the thermal conductivity ratio (TCR) of Al_2O_3-glycerol nanofluids, while the temperature has almost no significant effect on the data for range of this study. At room temperature, the effective thermal conductivity remains almost constant for 50 hours at 4% volume fractions. The comparison of the obtained experimental data and predictions from some existing theoretical and empirical models reveals that the thermal conductivity ratio and its trend could not be accurately explained by the models in open literature. Consequently, a new empirical correlation based on the experimental data has been developed in this study.

Keywords: Nanofluids, glycerol, thermal conductivity, volume fraction, alumina.

*Corresponding author: Prof. Mohsen Sharifpur

Tel: +27 12 420 2448 Email: mohsen.sharifpur@up.ac.za

Nomenclature

A_p	Projected area of nanoparticle, m^2
$circ$	Circularity
c_p	Specific heat, J/kg.K
d	Diameter, m
D	Einstein diffusion coefficient
F	F-statistic
h	Non-locality characteristic length, m
$\hbar$	Ratio, $\hbar = \frac{r}{h}$
k	Thermal conductivity, W/mK
K	A shape factor
p	p-value
P	Outline perimeter of nanoparticle, m
Pr	Prandtl number
r	Radius, m
R	Coefficient of correlation
Re	Reynolds number
SSA	Specific surface area, m^2
T	Temperature, ˚C
t	Time, s
$t_{v,p}$	Weighing function for ν degree of freedom and p % of probability
u	Uncertainty
u_B	Bias error
u_p	Precision or random error
wt.	Weight fraction of the species
W	Weight, kg

Greek symbols

β	Full-width at half maximum, rad
ε	Fraction of liquid volume that travels with a nanoparticle
θ	Diffraction angle, rad
κ	Boltzmann's constant, J/K
λ	X-ray wavelength, Å
μ	Viscosity, $N.s/m^2$
v	Velocity, m/s

$\Im 1$ Ratio, $\Im 1 = \frac{1}{\hbar} + \arctan(\hbar) - \frac{\pi}{2}$

$\Im 2$ Ratio, $\Im 2 = \arctan(\hbar) + \frac{\hbar}{1+\hbar^2} + \frac{8\hbar}{(1+\hbar^2)^2} + \frac{8\hbar^3}{(1+\hbar^2)^3} - \frac{\pi}{2}$

ρ Density, kg/m^3

σ_1 Ratio, $\sigma_1 = \left(1 + \frac{\delta}{r_p}\right)$

σ_2 Ratio, $\sigma_2 = \left(1 + \frac{\delta}{2r_p}\right)$

τ_D Time necessary for nanoparticle of diameter d_p to cover the distance equal to its size, s

ϕ Volume fraction

Subscripts

B	Brownian
$cryst$	Crystallite
eff	Effective
f	Fluid
fr	Freezing point of the base liquid
gly	Glycerol
p	Particle
TCR	Thermal conductivity ratio
10	10% of nanoparticles have diameter less than
50	Mean of particle diameter distribution
90	90% of nanoparticles have diameter less than

1. Introduction

The importance of heat transfer fluids with high thermal conductivity than conventional ones has been noted by many scientists and engineers since they improve the heat removal efficiency in heating or cooling systems. Experiments have shown that the suspended nanoparticles or nanofibers, viz. Cu, MgO, CuO, Al_2O_3, TiO_2, SiO_2, SiC, ZnO, graphene, carbon nanotube (CNT), multiwalled carbon nanotube (MWCNT) improve the transport and thermal properties of conventional fluids [1-8]. Experimental studies reveal the dependence of thermal conductivity ratio (TCR) of nanofluids on nanoparticles volume fraction, particles size, temperature, amount and type of surfactants, thermal conductivity of base fluid, thermal conductivity and size of nanolayer, aggregation, sedimentation time and pH of nanofluids. Numbers of experimental study [1, 9-11] have investigated the thermal conductivity of Alumina (Al_2O_3) nanoparticles prepared with different based fluids such as water, ethylene glycol, mixtures of ethylene glycol (EG) and water, oil, and methanol.

Recently, Ghanbarpour *et al.* [10] observed that the thermal conductivity of water based Al_2O_3 nanofluids increases non-linearly with nanoparticle concentration, but linearly with a rise of temperature. The nanoparticle of spherical shape and average size of about 75nm was investigated. The thermal conductivity enhancements were reported in the range of 1.1% to 87% at mass concentration ranging from 3% to 50% and temperature range of 20 ˚C to 50 ˚C. Mostafizur *et al.* [1] also measured the thermal conductivity of three different methanol based nanofluids for temperature ranging from 1˚C to 20 ˚C and volume fraction range of 0.005% to 0.15%. The sonication at frequency and power of 50Hz and 500 W, respectively were used for two hours to improve the dispersion of the mixture of Al_2O_3-methanol, SiO_2-methanol and TiO_2-methanol nanofluids with average particles diameter of 13, 5-15 and 21 nm, respectively. They found that the thermal conductivity of the nanofluids increased with a rise of nanoparticle volume fraction and temperature. Al_2O_3 nanoparticles dispersed in methanol gave greater enhancement of thermal conductivity than SiO_2 and TiO_2 nanoparticles, for the volume fraction range of 0.005% to 0.15%. At 20 ˚C, for 0.15% volume fraction of Al_2O_3, SiO_2 and TiO_2 nanoparticles, the thermal conductivity enhancement was 29.41%, 23.033% and 24.51% respectively.

Application of glycerol as anti-freeze in automotive applications is being examined by ASTM International Committee D15 [12]. In 1930's, glycerol was used as an anti-freeze before to be replaced by ethylene glycol due to cost considerations. Ethylene glycol is used as an anti-freeze for a wide variety of mechanical equipment during winter times to prevent freezing of aqueous heat-transfer fluids. Since 2004, there is a surplus production of glycerol from biodiesel in the global market. This situation could be favourable to make the glycerol cost effective as antifreeze. Glycerol is more environmental friendly than ethylene glycol. Moreover, it can remain fluid at low temperatures and resist to oxidation than oil. Glycerol is recommended when there is a contact with lubricant in food pharmaceutical, cosmetic manufacture and where mineral oils as lubricant are less recommended for oxygen compressor, pumps and bearings exposed to fluids such as gasoline and benzene [13].

There is a lack of information of α-Al_2O_3-glycerol nanofluids thermal conductivity in the literature. Therefore, this investigation is aimed to determine experimentally the impact of the nanoparticle volume fraction, particle diameter, temperature on the thermal conductivity of stable α-Al_2O_3-glycerol nanofluids. Additionally, the measured dataset were compared with the values predicted by some theoretical and empirical models of thermal conductivity of nanofluids, which may work for glycerol base nanofluids. Consequently, a new correlation of thermal conductivity of α-Al_2O_3-glycerol nanofluids is developed.

2. Material and Methods

2.1 Materials

Three α-Al_2O_3 nanoparticles of different diameters were analyzed in this work, which the manufacturer clam were 40 nm (S1), 80 nm (S2) and 100 nm (S3). The α-Al_2O_3 nano- powder of 80

nm was purchased from US Research Nanomaterials, Inc. (Houston, TX, USA). The 40 nm and 100 nm nanoparticles were procured from MK Nano, Inc. (Mississauga, ON, Canada). The glycerol (base fluid) was supplied by Merck Millipore (Darmstadt, Germany). Table 1 presents the physicochemical properties of the selected nanoparticles [14-16].

Table 1: Properties of Al_2O_3 nanoparticles

Item	Diameter (nm)	Purity (%)	Crystalline	Morphology	True Density (g/cm^3) at 20°C	Thermal conductivity (W/mK)
Al_2O_3	40	99.5	alpha	nearly spherical	3,7	40
Al_2O_3	80	99+	alpha	nearly spherical	3.5 – 3.9	40
Al_2O_3	100	99.9	alpha	nearly spherical	3,7	40

2.2 Physical characterization of nanoparticles

The physical characterisation of the α-Al_2O_3 nanoparticles were evaluated by using the X-ray Fluorescence Spectroscopy (XRF), X-ray powder Diffraction and the combined XRD and XRF, respectively. The XRF analyses were performed using an ARL 9400XP spectrometer. The XRD analysis of the prepared samples of α-Al_2O_3 nanoparticles samples was carried out on a PANanalytical X'Pert Pro powder diffractometer with Co-Kα radiation source (λ = 1.78901 Å) at 50 kV and current of 50 mA. The results were recorded over a 2 θ range of 10-90 ° with a scanning rate of 0.02°/s. Transmission Electron Microscopy (TEM) analysis of the samples was performed using JEM 2100F (JEOL, USA) to evaluate the shape and the size of particles. The JEM 2100F works with an accelerating voltage of 200 kV in the range of 50 V min at variable steps of 2 ppm/min. The JEM 2100F achieves the highest TEM images quality with point image resolution at 0.23 nm accuracy [17]. The TEM samples were prepared by dispersing the α-Al_2O_3 nano-powder in acetone, followed by ultrasonication of 5 minutes. TEM image files were analysed using ImageJ software (NIH, Bethesda, MD, USA).

2.3 Thermal conductivity measurement

The thermal conductivity of both glycerol and α-Al_2O_3-Glycerol nanofluid were measured with the KD2 Pro Thermal Properties Analyzer (Decagon device, USA). The handled device measure the thermal conductivity values ranging from 0.02 to 2 W/mK over the temperature range of 0 ˚C to 50 ˚C with 5% accuracy [18]. It works based on the transient short hot-wire source method. Several

researchers used successively the KD2 Pro [1, 19, 20]. The KD2 pro thermal analyser complies with both ASTM D5334 standard and IEEE 442-1981 regulations.

2.4 Preparation of nanofluids

The α-Al_2O_3-glycerol nanofluids were prepared in a 100 ml beaker with no surfactant for the volume fractions ranging from 0.5% to 4%. The nanofluid was ultrasonicated with S14 sonotrod (UP200S Hielscher of 200 Watts operated at 24 kHz) [21] for two hours to ensure uniform dispersion of the nanoparticles. A thermal bath (LAUDA ECO RE1225 Silver) was used to obtain and/or maintain different temperatures of nanofluids during the measurement process. After that, the nanofluids were kept still for 30 minutes to minimize the forced convection produced by both ultrasonicator probe and the thermal bath. The thermal bath LAUDA works in the temperature range from -5˚C and 200˚C at a minimum ambient temperature of 5˚C. It operates with a pump of maximum flow of 22 L/min and maximum pressure of 0.55 bar. A pump of maximum flow runs the heat transfer fluid in the thermal bath to maintain the required temperature of the nanofluid. The bath can contain a heat transfer fluid at minimum and maximum capacity of 9.3L and 12L, respectively [22]. Figure 1 shows the experimental set-up for thermal conductivity measurement.

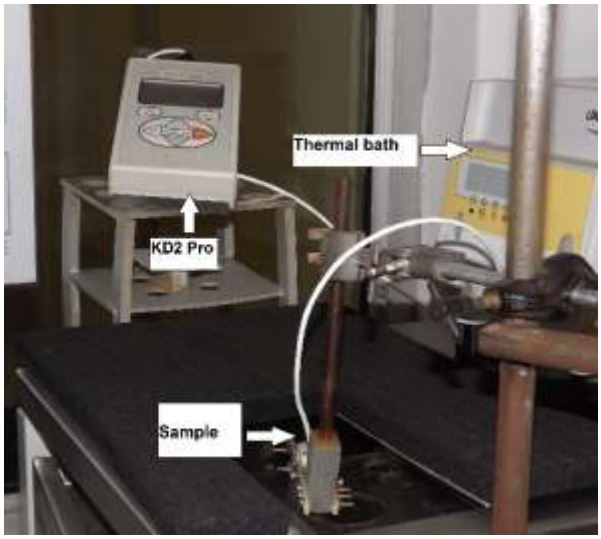

Figure 1: Experimental set-up for thermal conductivity measurement

The volume fraction of nanoparticles (ϕ) was determined using Eq. (1):

$$\phi = \frac{\frac{W_p}{\rho_p}}{\frac{W_p}{\rho_p} + \frac{W_{gly}}{\rho_{gly}}} * 100\% \quad (1)$$

where W_p, W_{gly}, ρ_p and ρ_{gly} are the weight of α-Al_2O_3 nanoparticles, the weight of glycerol, the density of α-Al_2O_3 nanoparticles and the density of glycerol, respectively. The nanoparticles, weighted by Adam electronic balance (model HCB1002), whose accuracy is 0.01g, were dispersed into the pre-weighed quantity of the base fluid.

2.5 Validation of experimental data

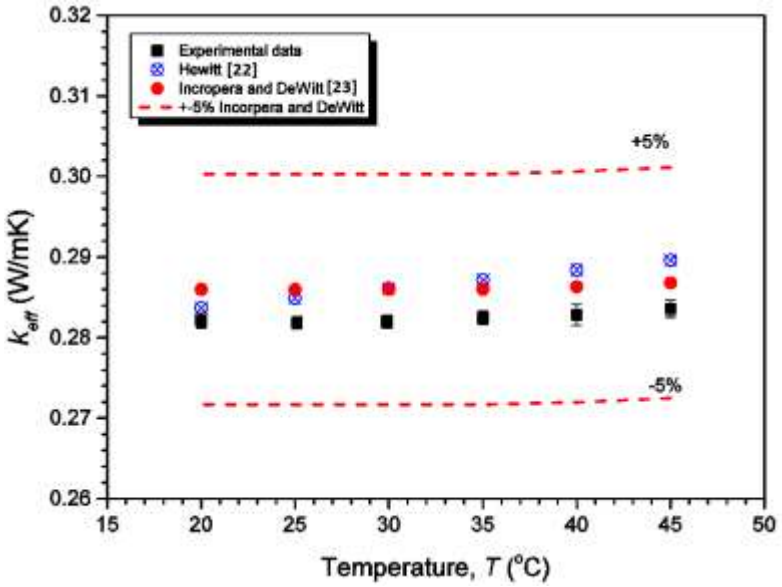

Figure **2** shows the values of thermal conductivity of glycerol measured with the KD2 Pro and the reference data for temperatures ranging from 20 ˚C to 45 ˚C [23, 24]. The reference values show a deviation of less than 1% between them. Each experimental data represents an average of nine measurements at various temperature. The results indicate that the measured data are in excellent agreement with available reference data, within ± 2% accuracy.

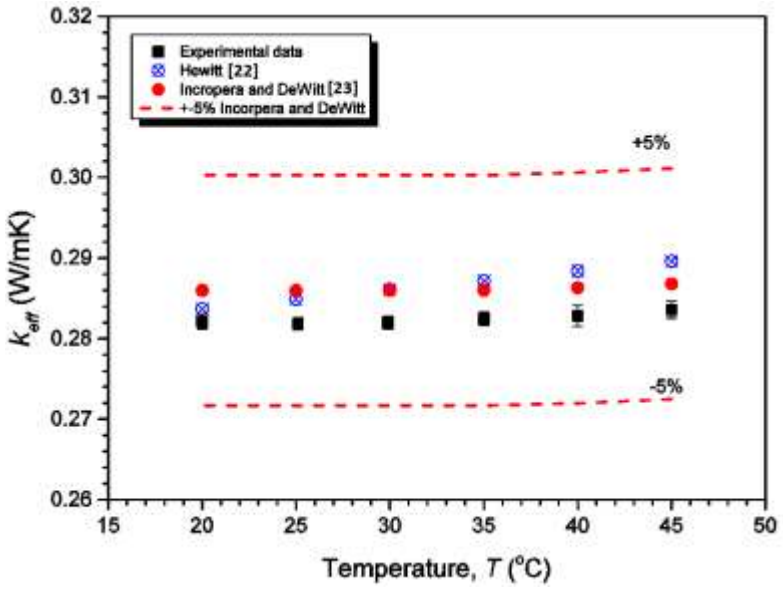

Figure 2 : Validation of experimental data

3. Results and Discussion

3.1 Sample characterization

Figure 3 shows the TEM images of the three samples of α-Al_2O_3 nanoparticles. Figure 4 (a) shows the particle size distribution of the α-Al_2O_3 nanoparticles determined using ImageJ software. The particle

size distribution is based on the TEM image analysis of more than 500 particles, which were individually counted.

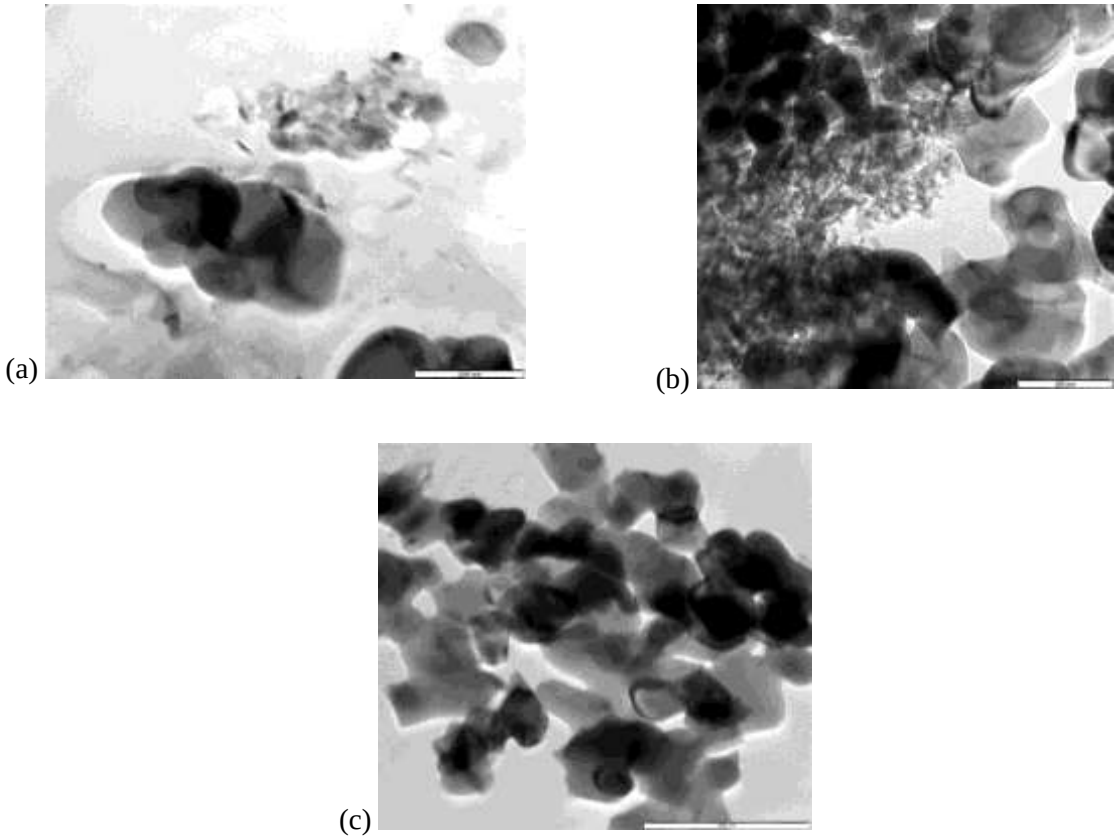

Figure 3: TEM image of α-Al_2O_3 nanoparticles (a) 31 nm, (b) 55 nm and (c) 134 nm

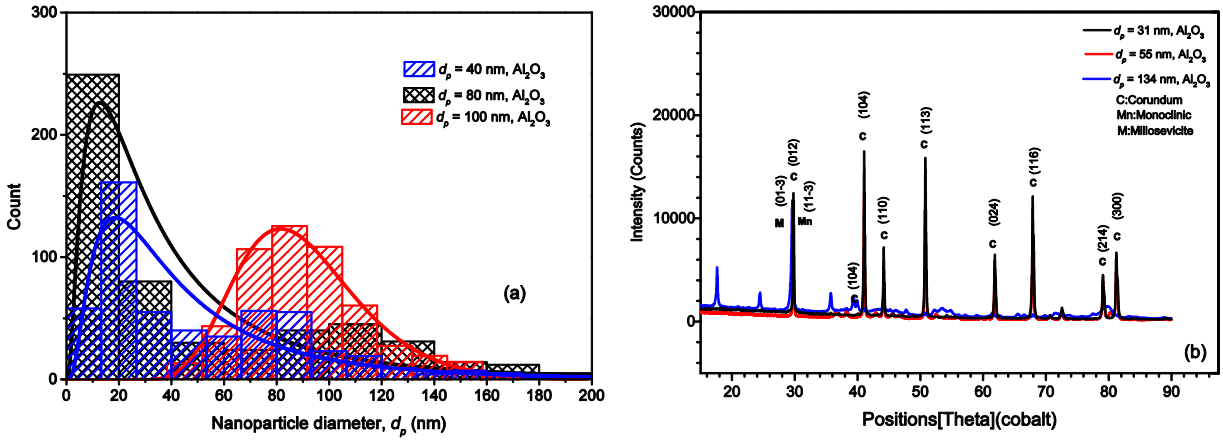

Figure 4: (a) Diameter distribution of α-Al_2O_3 nanoparticles (b) X-ray diffraction pattern of the α-Al_2O_3 nanoparticles powder

Both samples 1 and 2 show two prominent peaks bimodal data, each of its own with a separate central tendency while the sample S3 reveals an unimodal data distribution. The three α-Al_2O_3 nanoparticles show a positive skewed size distribution, in the range of 19 nm (d_{10}), 54 nm (d_{50}) and 155 nm (d_{90}) for the 40 nm, 12 nm (d_{10}), 21 nm (d_{50}) and 127 nm (d_{90}) for the 80 nm and 97 nm (d_{10}), 134 nm (d_{50}) and 187 nm (d_{90}) for the 100 nm, respectively [25, 26]. However, all the three nanoparticles respect the

lognormal distribution with the mean particle size respectively of 55 ± 2 nm for S1, 31 ± 3 nm for S2 and 134 ± 1 nm S3. There are significant differences in nanoparticles sizes between the obtained values and manufacture values. The situation may happen due to the unexpected event that can occur in the nanoparticle manufacturing process. As the manufacturer does not do the nanoparticle TEM analysis batch by batch to ascertain the size of produced nanoparticle. In this work, the obtained sizes are considered for further analyses i.e. 31 nm, 55 nm and 134 nm, respectively. Eq. (2) defines the circularity parameter ($circ$). The circularity of 1 and approaching 0 refers to the perfect circle and increasingly elongated shape object respectively [27].

$$circ = 4\pi \left(\frac{A_p}{P}\right)^2 \tag{2}$$

where A_p and P are the projected area and outside perimeter of the outline of the nanoparticle respectively.

The circularity of 31 nm, 55 nm and 134 nm α-Al_2O_3 nanoparticles are equal to 0.9. Thus, our nanoparticles have a shape close to the sphere than that of elongated shape object.

Figure 4 (b) shows XRD patterns of α-Al_2O_3 nanoparticles. The patterns are in good agreement with the standard diffraction data of two types of Al_2O_3 defined by the International Center for Diffraction Data (ICDD) database. The first one is Rho53

mbohedral system of Corundum (Al_2O_3) of Powder Diffraction Patterns with PDF file No. 01-089-7717 and the second Monoclinic Al_2O_3 (PDF file No. 01-086-1410) for 40 nm, a Rhombohedral system of Corundum (Al_2O_3) of PDF file No. 98-008-8029 for 80 nm and both Rhombohedral Corundum (PDF file No. 01-081-2267) and Rhombohedral Millosevichite (Al_2 $[SO_4]$)$_3$ of PDF file No. 01-077-0066 for 100 nm.

The mineralogical analysis confirms that both samples of S1 and S3 consist of a mixture of Corundum and Millosevichite, while S2 is composed of Corundum (Table 2 and Table 3). The crystallite size was estimated using Scherer equation (3). The equation (3) predicts at best ±10% the crystallite size which the assumption of K= 1 is considered [28].

$$d_{cryst} = \frac{K\lambda}{\beta \cos\theta} \tag{3}$$

where K is the shape factor varying from 0.62 to 2.08, λ is the wavelength of X-ray source, β is the peak width of the profile at Full Half Maximum Height (FWHM) of crystallite size and θ is the diffraction angle expressed in radian.

Table 2: Chemical composition of α-Al_2O_3 nanoparticles

Diameter	Al_2O_3	SiO_2	TiO_2	Fe_2O_3	MgO	CaO	Na_2O	P_2O_5	LOI*
40	99.7	0.02	0.00	0.04	0.16	0.01	0.02	0.02	0.3
80	99.88	0.02	0.36	0.06	0.2	0.01	0.02	0.09	0.40
100	74.28	0.02	0.03	0.05	0.13	0.01	0.05	0.02	26.86

*LOI: Loss of Ignition

The values of K are 0.89 and 0.94 for a spherical particle with cubic symmetry crystallites determined by integral breadth and FWHM, respectively [29, 30]. K can take an approximate value of one in both situations [31]. The average crystalline sizes are 38.0 nm for the 33 nm α-Al_2O_3, 48.4 nm for 55 nm α-Al_2O_3 and 35.4 nm for 134 nm α-Al_2O_3 nanoparticles, respectively. However, the calculation has been done without correction for instrumental, stress broadening and any other possible sources of line broadening**.**

Table 3: Mineralogical composition of α-Al_2O_3 nanoparticles

Mineral	**Nanoparticles**					
	40 nm α-Al_2O_3		80 nm α-Al_2O_3		100 nm α-Al_2O_3	
	Weight (%)	3 SD	Weight (%)	3 SD	Weight (%)	3 SD
Millosevichite (Al_2SO_4)	19.5		0	0	-	
Corundum (Al_2O_3)	80.5		100	0	-	

3.2 Uncertainty calculation

The uncertainty of experimental results was determined from both the bias error (instrument) and precision error resulting from the deviation in the experimental dataset. The bias error in measurement of thermal conductivity by KD2 Pro is 5%. The accuracy of the weighing scale is 0.01g. The uncertainty of the experiment is obtained by the following [32]:

$$u = \pm\sqrt{(u_B)^2 + (u_P)^2} \tag{4}$$

with $$u_p = \pm t_{v,p} SD$$

where u_B, u_p, $t_{v,p}$ and SD are bias error, precision or random error in measurement with p% probability, weighing function for v degree of freedom and p% probability and sample standard deviation, respectively. The uncertainty in TCR (u_{TCR}) is given as follow:

$$u_{TCR} = \left[\left(\frac{\delta k_{eff}}{k_f}\right)^2 + \left(\frac{-k_{eff}}{[k_f]^2}\delta k_f\right)^2\right]^{0.5} \tag{5}$$

where δk_{eff} and δk_f are uncertainty at $p\%$ probability including both bias and precision errors associated with the measured effective thermal conductivity of nanofluids and thermal conductivity of nanofluids, respectively. Finally, the uncertainty in the effective thermal conductivity and TCR was found to be between 5.1 % and 8.5%.

3.3 Experimental study of thermal conductivity

3.3.1 Introduction

The impact of parameters is statistically analyzed based on 72 data of TCR variability. A linear regression analysis is performed in each of the following sections to evaluate the individual impact of each parameters on the TCR, assuming the other variables are held constant, whereas a multivariate analysis will be performed to calculate if the independent variables jointly can influence the TCR. The F and t-ratio tests are used to for regression analysis [33, 34].

3.3.2 Effect of particle volume fraction and particle diameter

Figure 5 shows the effect of particle volume fraction (at volume fractions of 0.5%, 1%, 2% and 4%, respectively) on the effective thermal conductivity ratio of three sizes of α-Al_2O_3-glycerol nanofluids at 20 °C. The α-Al_2O_3 nanoparticles dispersed in glycerol yielded higher thermal conductivity than the base fluid (glycerol). As it is obvious in the figure, effective thermal conductivity increases linearly with an increase of volume fraction for each particle size. A linear regression analysis is performed to determine the effect of volume fraction on the TCR. The equation (6) obtained has R^2 of 0.822 and F-statistic of the model is 322.8 which correspond to significance p of 0.000. It means that the model is statistically significant and 82.2% of the variability in the TCR values is explained by the model. The rest (17.8%) of variation in TCR can be explained by residual and other variables.

$$\frac{k_{eff}}{k_f} = 0.997 + 3.824\phi \tag{6}$$

where ϕ is the α-Al_2O_3 nanoparticle volume fraction.

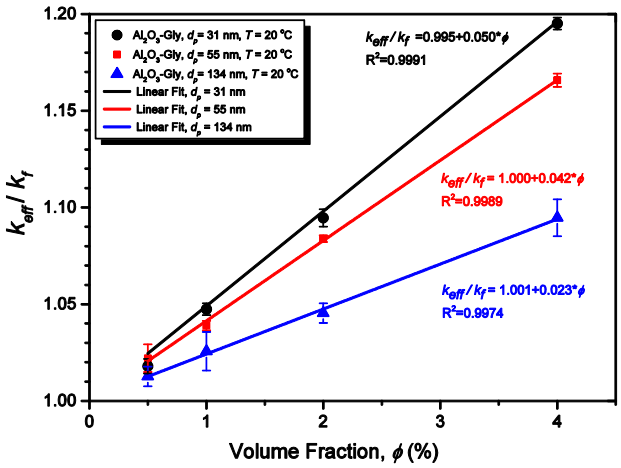

Figure 5: Influence of the Nanoparticle volume fraction on the thermal conductivity ratio of the three set of α-Al_2O_3-glycerol nanofluids at 20 °C

There is a linear increase of TCR with increase of α-Al_2O_3 nanoparticles volume fraction. This outcome is in agreement with other studies for various types of nanofluids [35-40]. The thermal conductivities ratio improved up to 19.5%, 16.6% and 9.5% at nanoparticle volume fraction of 4% for 31 nm, 55 nm and 134 nm size nanoparticles, respectively. Figure 5 clearly depicts the impact of particle size on the TCR. Smaller particles size lead to high thermal conductivity of nanofluids than the bigger ones. The same situation have been perceived at various range of temperature.

The estimated straight-line regression of TCR on diameter (size) is given by equation (7).

$$\frac{k_{eff}}{k_f} = 1.0997 - 4.29 \times 10^{-4} d_p \quad (7)$$

where d_p is the particle diameter in nm.

The equation (7) has R^2 of 0.111 and the F-statistic of the model is 8.78 which correspond to significance p of 0.004 ($p < 0.05$). It means that 11.1% of the variability in the TCR values is explained by the model. The rest (88.9%) of variation in TCR can be explained by residual, volume fraction and other variables. The t-ratio of intercept and slope (diameter) are 88.816 and - 2.963, respectively. Their correspondent significant p-values are 0.000 and 0.004 ($p < 0.05$). Therefore, the model is statistically valid. The thermal conductivity ratio of α-Al_2O_3-glycerol nanofluids increases with decreasing particle size for each volume fraction and temperature. These variation could be explained by the Brownian motion.

The improvement of thermal conductivity ratio in all the three nanofluids with respect to volume fraction could be possibly be explained by one or more mechanisms including Brownian motion, nanoparticles clustering, layering at the solid-liquid interface.The suspended α-Al_2O_3 nanoparticles in the glycerol increase the surface area and the heat capacity of the glycerol, and both interaction and collision among α-Al_2O_3 nanoparticles are strengthened [41, 42]. The Brownian diffusion coefficient (D) is expressed by Einstein-stokes equation [43] as follow:

$$D = \frac{\kappa T}{3\pi \mu_f d_p} \quad (8)$$

where κ is the Boltzmann constant (J/K), T is the temperature of the nanofluid (K), μ_f is the viscosity of the base fluid (N/s.m^2) and d_p is the nanoparticle diameter (m).

Einstein-stoke equation (8) shows that the nanofluids prepared with smaller size nanoparticles will result in high D coefficient than the one prepared with bigger size. Consequently, more severe collisions among nanoparticles and fluid molecules will be present in nanofluids which lead to better thermal conduction [44, 45]. The increase of particle volume fraction decreases the distances between nanoparticles in nanofluids. This phenomenon associated with severe collision into nanofluids lead to better thermal conduction [41]. Moreover, smaller particles exhibit larger surface area to volume ratio

than the bigger particles, which can possibly result in noticeable enhancement of the effective thermal conductivity [5].

3.3.3 Effect of temperature

Figure 6 (a) shows the effect of temperature on the effective thermal conductivity of 31 nm α-Al_2O_3-glycerol nanofluids for three different sizes of nanoparticles. The results observed in Figure 6 (a) depict that the temperature dependence of the effective thermal conductivity of nanofluids tracks the base fluid (glycerol), but in another level of magnitude. Analogous results were observed for 55 nm and 134 nm α-Al_2O_3-glycerol nanofluids. Similar findings were reported for the Al_2O_3-water nanofluids [38], and Ethylene Glycol based nanofluids containing Al_2O_3, MgO, ZnO, SiO_2, and graphene nanoparticles [5, 10, 38, 46].

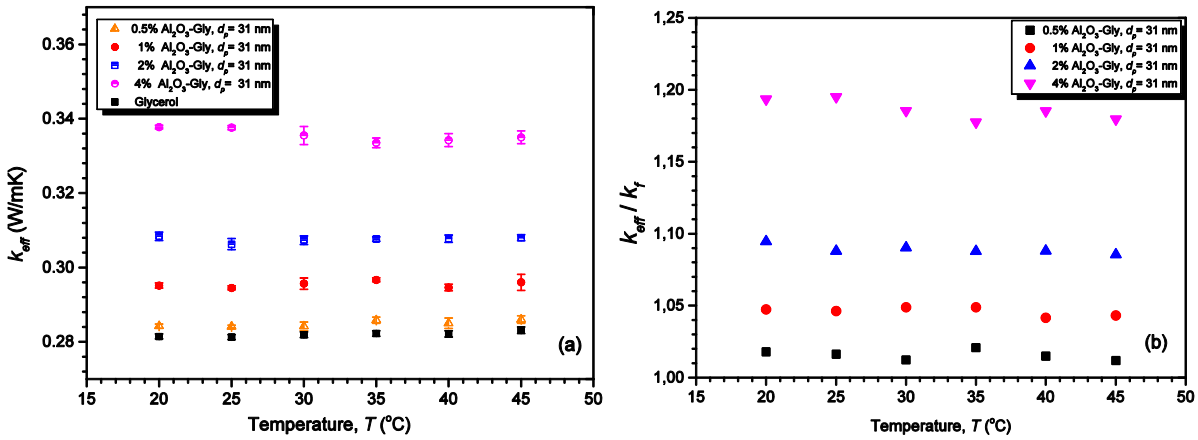

Figure 6: Temperature dependence of 31 nm α-Al_2O_3-glycerol nanofluids at different volume concentrations (a) Effective thermal conductivity (b) Thermal conductivity ratio

Figure 6 (b) shows the thermal conductivity ratio of 31 nm α-Al_2O_3-glycerol nanofluids at different volume fractions as function of temperature. The estimated line relationship between the temperature and the TCR computed is as follow.

$$\frac{k_{eff}}{k_f} = 1.071 - 7.02 \times 10^{-5} T \quad (9)$$

where T is temperature expressed in ˚C.

The obtained equation has unadjusted R^2 = 0.0001, F = 0.01 and significant p = 0.930 (p > 0.05); which is obviously greater than the significance level 0.05. The t-ratio of intercept and slope (temperature) are 39.87 and - 0.09, respectively. Their correspondent significant p value are 0.000 (p < 0.05) and 0.930 (p > 0.05). Thus, there is no significant dependence of TCR with temperature for the glycerol based α-Al_2O_3 nanofluids. The founding are in agreement with results obtained by Xie *et al.* for both 5% Fe_3O_4-kerosene and 1% MgO-EG nanofluids over the temperatures ranging from 10 ºC to 60 ˚C [47, 48]. They revealed that the effective thermal conductivity of both 5% MgO-EG and 1% Fe_3O_4-kerosene nanofluids vary, while the (k_{eff} / k_f) are almost constant. On contrary, Saleh *et al.*

[19] recently and also some others [10, 19, 35, 44, 45] depict that the effective thermal conductivity ratio of nanofluids varies with increase in temperatures. Therefore, it can conclude that the effect of temperature on thermal conductivity ratio depends on the nanofluids characteristics. Figure 6 (a) and (b) show that the thermal conductivity of α-Al_2O_3-glycerol nanofluids varies significantly with increasing of ϕ and decreasing of d_p as well. For all the three nanofluids samples, the thermal conductivities ratio improved up to 19.5%, 16.6% and 9.5% for Al_2O_3-α nanoparticle volume fraction of 4% for 31 nm, 55 nm and 134 nm size nanoparticles, respectively at 20˚C.

3.3.4 Stability of α-Al_2O_3-glycerol nanofluids

Figure 7 shows the stability of the α-Al_2O_3-glycerol nanofluids evaluated for 4% volume fraction. Thirty minutes after sonication, the effective thermal conductivity was acquired for all three nanoparticles sizes at 1 hour step, up to 50 hours. The t-statistic of the slope of the model (Eq. 10) of effective thermal conductivity of the model vs. elapsed time after preparation is 0.175. The R-square and p-value of both the F and t statistics are 0.000 and 0.861 (> 0.05), respectively. The variation of effective thermal conductivity of the model vs. elapsed time after preparation is not statistically justified. There is no dependence of k_{eff} of the model with elapsed time up to 50 hours. The best model is the naïve model, which is the mean value of k_{eff}. The mean values and standard deviation are 0.335 ±0.002 W/mK, 0.331±0.001 W/mK and 0.304±0.001 W/mK for 31 nm, 55 nm and 134 nm, respectively.

$$k_{eff} = 0.323 - 3.66 \times 10^{-9} t \tag{10}$$

where t is elapsed time in second.

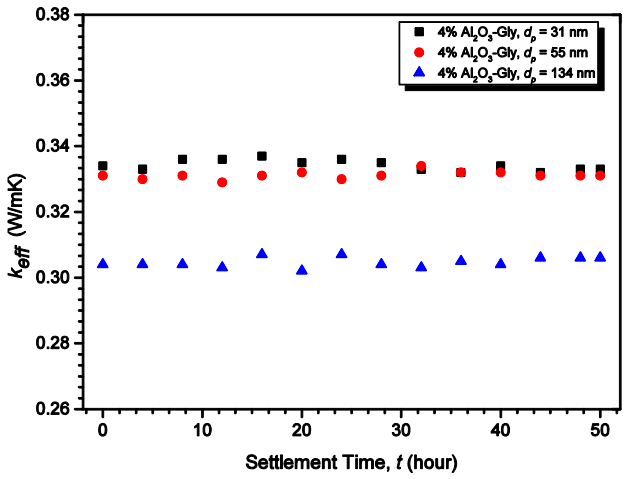

Figure 7: Influence of Settlement time on the Effective thermal conductivity of 4% α-Al_2O_3-glycerol nanofluids

The possible explanation of no enhancement of thermal conductivity of α-Al_2O_3-glycerol nanofluids in the early hours after sonication could be the no clustering and settling of nanoparticles [41, 47, 49, 50].

The effective thermal conductivity measurement indicates the stability of α-Al_2O_3-glycerol nanofluids at room temperature for at least 50 hours after preparation.

3.4 Comparison of the thermal conductivity models with experimental data

3.4.1 Existing theoretical and empirical models

Numerous studies, both experimental and theoretical, have been conducted to estimate the effective thermal conductivity of different nanofluids [51]. Several mathematical models of effective thermal conductivity of nanofluids have been proposed. This section presents the comparisons between the experimental data of α-Al_2O_3-glycerol nanofluids and predictions from some existing theoretical models. Maxwell [52] offered the first and simple model of effective thermal conductivity for micro or millimetre sized spherical particles suspended in base fluids as follows:

$$\frac{k_{eff}}{k_f} = \frac{k_p + 2k_f + 2(k_p - k_f)\phi}{k_p + 2k_f + (k_p - k_f)\phi} \tag{11}$$

where k_p , k_f and ϕ are the thermal conductivity of particle, the thermal conductivity of the base fluid, and the volume fraction of suspension, respectively. Maxwell's formula (Eq. 11) gives a good result for well-dispersed non-interacting spherical-shaped particles with low particle volume concentrations (less than 1% [51]) and negligible thermal resistance at the particle-fluid interface.

Shaker *et al*. [53] recently proposed an extended Maxwell model as Eq. (12) for the thermal conductivity of nanofluids. They modify the classical model of Maxwell by taking into account for the nonlocal heat transfer rising due to the small characteristic length in nanofluids. The non colinearity parameter (h) is determined by comparison between the novel model predictions and the experimental data of each given nanofluids. They depicted that h is equal to 8 and 11 for alumina-EG and alumina-water nanofluids, respectively. The model is valid for spherical nanoparticles suspended in base fluid and can be modified to account also for not spherical nanoparticles suspension.

$$\frac{k_{eff}}{k_f} = \frac{1 + 2\xi\phi\hbar^{-3}}{1 - \xi\phi\hbar^{-3}} \tag{12}$$

with

$$\xi = \frac{k_p - k_f}{3(\Im 1 k_p - \Im 2 k_f)} \tag{13}$$

$$\Im 1 = \frac{1}{\hbar} + \arctan(\hbar) - \frac{\pi}{2} \tag{14}$$

$$\Im 2 = \arctan(\hbar) + \frac{\hbar}{1+\hbar^2} + \frac{8\hbar}{(1+\hbar^2)^2} + \frac{8\hbar^3}{(1+\hbar^2)^3} - \frac{\pi}{2} \tag{15}$$

$$\hbar = \frac{r}{h} \tag{16}$$

Aybar et al. [54] reported the Bruggeman correlation which is implicit formula for the effective thermal conductivity of spherical particles randomly distributed in the base fluid. The model is based on the differential effective medium (DEM) theory to estimate the effective thermal conductivity of composites at low and high particle volume concentrations. The model predicts good match with some experiment results for low and high solid concentration when the particle size is not a concern. This model gives the same result as the Maxwell model provides for low solid concentration, while the effect of size has not considered.

$$\phi\left(\frac{k_p - k_{eff}}{k_p + 2k_{eff}}\right) + (1-\phi)\left(\frac{k_f - k_{eff}}{k_f + 2k_{eff}}\right) = 0 \tag{17}$$

R.S. Vajjha and D.K. Das [39] offer a relation which is an improvement of the Koo and Kleinstreuer model derived from a broader set of data (133 data points), obtained from three nanofluids, viz. Al_2O_3, CuO and ZnO prepared with a mixture of water and 60:40 (by mass) ethylene. The model incorporates the classical Maxwell model and the Brownian motion effect to account for the thermal conductivity of nanofluids as a function of temperature, particle volumetric concentration, the properties of the nanoparticles and the base fluid. The applicable range is at temperature of 298-363 K and 29-77 nm for the particle size, respectively. The proposed equation is

$$k_{eff} = k_{eff,Maxwell} + 5x10^4 \epsilon \phi \rho_p c_{pf} \sqrt{\frac{\kappa T}{\rho_p d_p}} f(T,\phi) \tag{18}$$

where the function $f(T,\phi)$ in Eq. (19) is the same for all three nanofluids as:

$$f(T,\phi) = (2.8217 \times 10^{-2}\phi + 3.917 \times 10^{-3})\left(\frac{T}{T_0}\right) - (3.0669 * 10^{-2}\phi + 3.91123 \times 10^{-3}) \tag{19}$$

The ϵ correlation is the same for Al_2O_3 and ZnO but differs for CuO:

$\epsilon = 8.4407(100\phi)^{-1.07304}$ (20) for Al_2O_3 for $1\% < \phi < 10\%$ and ZnO for $1\% < \phi < 7\%$;

$\epsilon = 9.881(100\phi)^{-0.9446}$ (21) for CuO for $1\% < \phi < 6\%$

The effective medium equation [38] which introduce as Eq. (22), predicts the thermal conductivity ratio for highly conducting spherical particles. In the model, the particles are assumed to be immobile which cannot be realistic.

$$k_{eff} = [1 + 3\phi]k_f \tag{22}$$

Corcione [55] developed an empirical correlation as Eq. (23) for predicting the thermal conductivity ratio from experimental data, consisting of alumina, copper oxide, titania and copper nanoparticles suspended in water or ethylene glycol (EG). The correlation is valid for nanoparticle in the range of temperatures 21-51˚C, volume fraction 2-9% and nanoparticle diameter 10-150 nm. The correlation was obtained by the way of regression analysis with a 1.86% standard deviation of error. The water and EG thermal conductivity are 0.598 W/m.˚C and 0.237 W/m.˚C, respectively at 20 ˚C. The glycerol thermal conductivity is 0.2837 W/m.˚C, which is between them [23, 24]. Thus, the k_{eff} of Glycerol based nanofluids may predict by Corcione correlation.

$$\frac{k_{eff}}{k_f} = 1 + 4.4Re_p^{0.4}Pr_f^{0.66}\left(\frac{T}{T_{fr}}\right)^{10}\left(\frac{k_p}{k_f}\right)^{0.66} \tag{23}$$

where Re_p is the nanoparticle Reynolds number, Pr_f is the Prandtl number of the base fluid, T is the nanofluid temperature, T_{fr} is the freezing point of the base liquid in Kelvin, k_p is the nanoparticle thermal conductivity and ϕ is the volume fraction of the suspended nanoparticles.

with

$$Re = \frac{2\rho_f \kappa T}{\pi \mu_f d_p} \tag{24},$$

$$Pr = \frac{\mu_f C_{pf}}{k_f} \tag{25}$$

Li and Peterson [56] developed a correlation by linear regression analysis for predicting the thermal conductivity of Al_2O_3-distilled water nanofluids. The Al_2O_3 nanoparticles of the average diameter of 36 nm were mixed with water at volume fraction range of 2% to 10% for Al_2O_3 and temperature range of 28.9 ˚C to 33.4 ˚C. They depicted that the particle volume fraction dependence of the effective thermal conductivity is much higher than the temperature dependence as well as the volume fraction dependence is more pronounced with increasing temperature.

$$\frac{\left(k_{eff} - k_f\right)}{k_f} = 0.764481\phi + 0.018688867T - 0.462147175 \tag{26}$$

3.4.2 Comparison between existing models and experimental data

Figure 8 provides the comparison of the predicted effective thermal conductivity ratio from various models (Maxwell, Bruggeman, Effective medium theory, Vajjha *et al.*, Li and Peterson, Corcione and Shaker) with experimental data of three sizes of α-Al_2O_3-glycerol nanofluids versus volume fraction at room temperature. Li and Peterson model under-predictn the experimental data of 31 nm and 55 nm α-Al_2O_3-glycerol nanofluids whereas Vajjha *et al*. model over-predicts range for ϕ < 4% (see Figure 8

(a) and (b)). Corcione model shows a slight increase of TCR with ϕ compared the experimental data. However, the increasing ϕ results in the diversion of Corcione model from experimental data. The other models give a good match to experimental data for ϕ < 2%. Figure 8 (c) discloses more or less similar results as exposed in Figure 8 (a) and (b), with the exception of both Shaker models, Maxwell, Li and Peterson, Bruggeman and Effective medium model are slightly higher than the experimental data of 134nm α-Al_2O_3-glycerol nanofluids for ϕ > 2%.

Figure 9 (a), (b) and (c) present a comparison of the predicted TCR versus temperature for the selected models with experimental data of 31 nm, 55nm and 134nm α-Al_2O_3-glycerol nanofluids prepared at 4% volume fraction. Corcione model under-predicts the experimental results of the three α-Al_2O_3-nanofluids. Li and Peterson model give good results for temperature for a part of temperature range (between 25 ˚C to 30 ˚C for 134 nm and between 30 ˚C to 35 ˚C for 31 nm and 55 nm). Vajjha model gives good predictions for temperature less than 30˚C for 31 nm and temperature more than 35 ˚C for 55 nm. However, all the three previous models increase with the temperature rise disagreeing with the expected trend. The other models follow the expected trend and predict values that are lower than the experimental data for both 31 nm and 55 nm and greater than the experimental data for 134 nm.

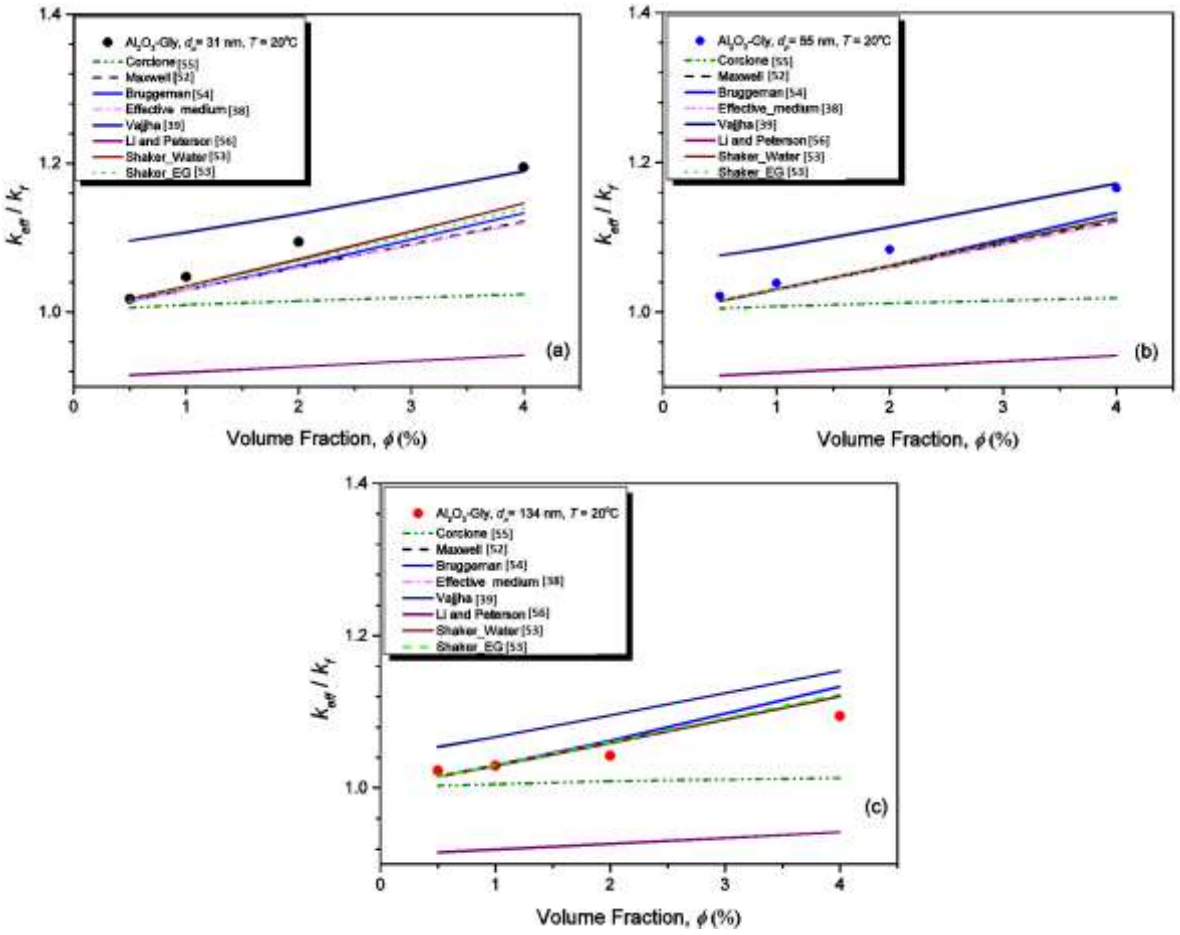

Figure 8: Comparison of the thermal conductivity ratio variation with volume fraction between the predictions form selected models and experimental data for α-Al_2O_3-glycerol nanofluids at 20˚C: (a) 31 nm, (b) 55 nm and (c) 134 nm

Figure 10 provides comparisons of the predicted TCR versus diameter relationship for the selected models with experimental data sets of α-Al_2O_3-glycerol nanofluids prepared at 4% volume fraction. Corcione underestimate the experimental data set while Vajjha model overestimate. The TCR of α-Al_2O_3-glycerol nanofluids agrees well with the prediction of Maxwell, Bruggeman and effective medium, but their trend is contrary to the expected one. Li and Peterson model overestimated the TCR for the three nanofluids. Its pattern is dissimilar to the experimental data trend.

Although the prediction of certain selected models are partially within the acceptable range of experimental data of α-Al_2O_3-glycerol nanofluids for the various involved parameters, (see Figure 8, Figure 9 and Figure 10), but the models trend didn't follow the expected trend for each analyzed parameter (temperature, size and volume fraction) while the models underpredict or overpredict the experimental data or the model trend doesn't follow the data pattern.

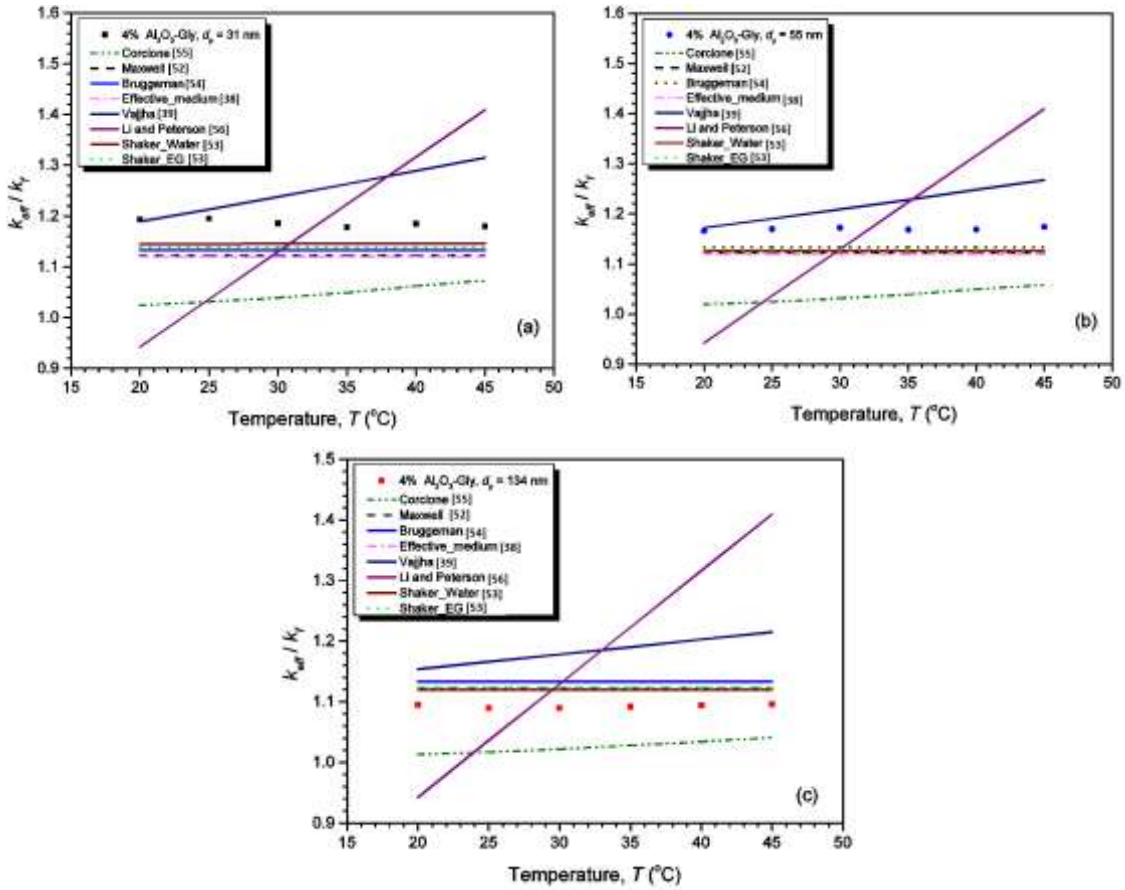

Figure 9: Comparison of thermal conductivity ratio variation with temperature between the predictions form selected models and experimental data for 4% α-Al_2O_3-glycerol nanofluids: (a) 31 nm, (b) 55 nm and (c) 134 nm

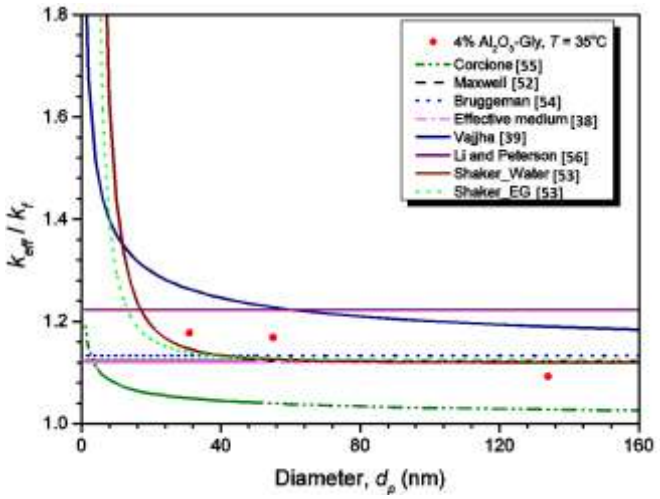

Figure 10: Comparison of thermal conductivity ratio variation with nanoparticle diameter between the predictions form selected models and experimental data for 4% α-Al_2O_3-glycerol nanofluids at 35˚C

3.4.3 New empirical correlation for the thermal conductivity ratio of α-Al_2O_3-glycerol nanofluids

A new empirical correlation is derived from the experimental data on α-Al_2O_3-glycerol nanofluids over the temperature range 20 ˚C to 45 ˚C, concentration range 0.5% to 4% and particle sizes (d_p) ranging from 31nm to 134 nm. The novel equation is a modified version of Corcione model [55]. The relationship between the TCR (dependent variable) and the independent variables are statistically verified by regression analysis [33]. Eq. (27) is the developed empirical correlation for α-Al_2O_3-glycerol nanofluid.

$$\frac{k_{eff}}{k_f} = 1 + Re_p^{0.4377} Pr_f^{0.9400} \phi^{1.0475} \left(\frac{k_p}{k_f}\right)^{0.6661} \quad (27)$$

where k_p is the thermal conductivity of the α-Al_2O_3 nanoparticles (equal to 40 W/mK). The others parameters are defined in section 3.4.1.

Equation (27) has unadjusted R-square = 0.980, F = 3.7*10^5 and significant p = 0.0000. The t-statistic of Re_p, Pr_f, ϕ and k_p / k_f exponents are 19.4, 20.3, 38.5 and 16.1, respectively. Their associated p-values are highly significant (p < 0.001). No colinearity exists between exploratory parameters as their variance inflation factor (VIF) < 10. However, the p-value of the independent term of the equation and the exponents of both Prandtl number and temperature were not statistically significant in the general Corcione model. After exclusion of the temperature term (T / T_{fr}), the multicollinearity remains due to high linear correlation (R = 0.9992) between the k_p / k_f and the independent terms of the equation. The comparison between the predicted TCR from the new correlation and the experimental data shows an excellent agreement with maximum relative error of -2.37%, and the average relative error of -

0.03% (see Figure 11). Also, the residual sum is zero and there is no autocorrelation in the residuals. The offered analysis provides evidence that the new model is statistically significant.

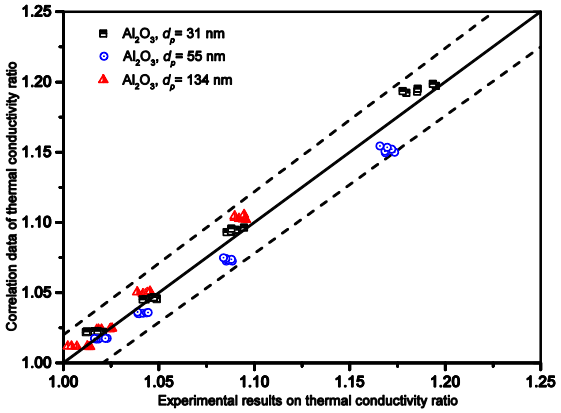

Figure 11: Comparison of the thermal conductivity ratio between the predicted values from the new correlation and the experiments data on α-Al_2O_3-glycerol nanofluids

Figure 12 depicts the impact of temperature on the three standardized parameters of the novel equation for α-Al_2O_3-glycerol nanofluid. The standardized parameters are Reynolds number term $Re^{0.4377}$, Prandtl number term $Pr^{0.9400}$ and thermal conductivity of nanoparticle normalised to the thermal conductivity of glycerol term $[k_p \,/\, k_f]^{0.6661}$. Figure 12 discloses that the standardised Pr decreases with a rise in temperature while the standardized Re increases and standardized term $k_p \,/\, k_f$ is almost unchanged. The magnitude of Pr term is much larger compared to combined Re and standardized $k_p \,/\, k_f$terms. The normalized Pr is the major parameter describing the enhancement of TCR of α-Al_2O_3-glycerol nanofluids, as opposed to the Reynold number for the case of Al_2O_3-water nanofluid [57]. The described phenomenon strengthens the TCR with the rise of volume fraction of suspended α-Al_2O_3 nanoparticle in the glycerol.

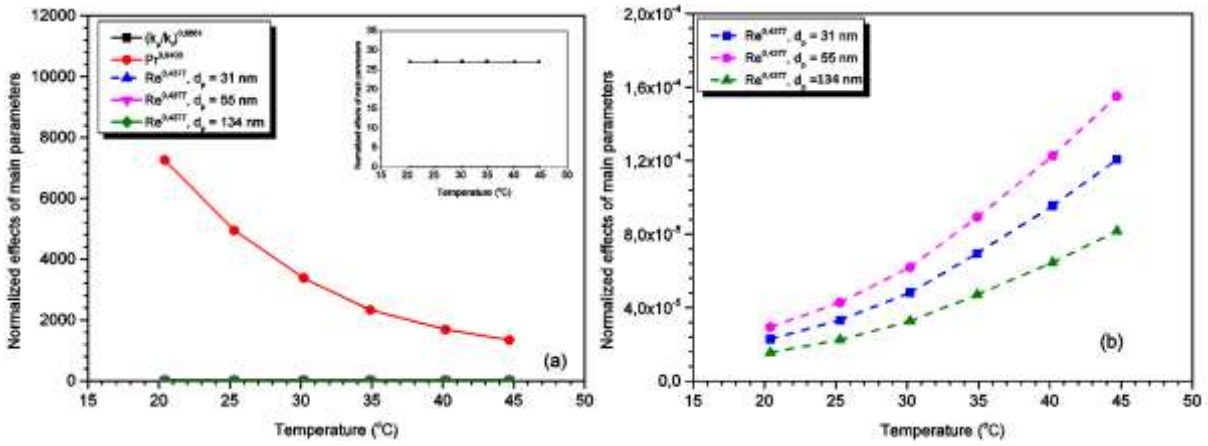

Figure 12: Temperature dependence of the effects of the novel correlation of 1% volume fraction α-Al_2O_3-glycerol nanofluids of (a) the three parameters of (b) Re parameters

4. Conclusion

The following findings are drawn from the experimental results and discussions on the thermal conductivity of α-Al_2O_3-glycerol nanofluids:

1. The addition of α-Al_2O_3 nanoparticles to glycerol (base fluid) enhances the effective thermal conductivity of glycerol. However, the effective thermal conductivity of nanofluid tracks the base fluid, but shifted.
2. The thermal conductivity ratio increases linearly with volume fraction of α-Al_2O_3 nanoparticles at a constant temperature. It is unchanged with temperature variation. The TCR decreases with increasing of nanoparticle's size under the condition of the same volume fraction and temperature.
3. The α-Al_2O_3-glycerol nanofluids prepared without any surfactants can stay stable for at least 50 hours after preparation.
4. The Prandtl number is the major parameter describing the enhancement of TCR of α-Al_2O_3-glycerol nanofluids, not the Reynold number. The impact of Brownian diffusion is minor compared to the thermal diffusion in the thermal conductivity enhancement of the α-Al_2O_3-glycerol nanofluids.
5. The predictions from models in the literature are partially within the acceptable range of experimental data for the various involved parameters, but either didn't follow the expected pattern for each analyzed parameter (temperature, size and volume fraction) or are not consistent in all conditions.
6. Therefore, a new empirical correlation has been developed.

Acknowledgements

The authors from University of Pretoria, gratefully acknowledge the funding obtained from Energy IRT Seed-funding (2014-EIRTSharifpur).

References

[1] R.M. Mostafizur, M.H.U. Bhuiyan, R. Saidur, A.R. Abdul Aziz, Thermal conductivity variation for methanol based nanofluids, International Journal of Heat and Mass Transfer, 76 (2014) 350-356.

[2] K.S. Suganthi, K.S. Rajan, A formulation strategy for preparation of ZnO–Propylene glycol–water nanofluids with improved transport properties, International Journal of Heat and Mass Transfer, 71 (2014) 653-663.

[3] A.N. Al-Shamani, M.H. Yazdi, M. Alghoul, A.M. Abed, M. Ruslan, S. Mat, K. Sopian, Nanofluids for improved efficiency in cooling solar collectors–A review, Renewable and Sustainable Energy Reviews, 38 (2014) 348-367.

[4] M.J. Pastoriza-Gallego, L. Lugo, D. Cabaleiro, J.L. Legido, M.M. Piñeiro, Thermophysical profile of ethylene glycol-based ZnO nanofluids, The Journal of Chemical Thermodynamics, 73 (2014) 23-30.

[5] H. Xie, W. Yu, Y. Li, L. Chen, Discussion on the thermal conductivity enhancement of nanofluids, Nanoscale Research Letters, 6(1) (2011) 1-12.

[6] V. Bianco, O. Manca, S. Nardini, K. Vafai (Eds.), Heat Transfer Enhancement with Nanofluids, CRC Press, Boca Raton Fl, USA, 2015, ISBN 9781482254006.

[7] K. Khanafer, K. Vafai, A critical synthesis of thermophysical characteristics of nanofluids, Int. J. Heat Mass Transf. 54 (2011) 4410-4428.

[8] B. Buonomo, O. Manca, L. Marinelli, S. Nardini, Effect of temperature and sonication time nanofluid thermal conductivity measurements by nano-flash method, Applied Thermal Engineering, 91, (2015) 181-190.

[9] J. Lee, K. Han, J. Koo, A novel method to evaluate dispersion stability of nanofluids, International Journal of Heat and Mass Transfer, 70 (2014) 421-429.

[10] M. Ghanbarpour, E. Bitaraf Haghigi, R. Khodabandeh, Thermal properties and rheological behavior of water based Al2O3 nanofluid as a heat transfer fluid, Experimental Thermal and Fluid Science, 53 (2014) 227-235.

[11] L. Syam Sundar, E. Venkata Ramana, M.K. Singh, A.C.M. Sousa, Thermal conductivity and viscosity of stabilized ethylene glycol and water mixture Al2O3 nanofluids for heat transfer applications: An experimental study, International Communications in Heat and Mass Transfer, 56 (2014) 86-95.

[12] ASTM, Proposed ASTM Engine Coolant Standards Focus on Glycerin, 2010. Available: http://www.astmnewsroom.org/default.aspx?pageid=2115. [Online, accessed: 14 April 2014].

[13] SDA, Glycerine-An Overview, The Soap and Detergent Association, Glycerine and Oleochemical Division, 1990. Available: www.aciscience.org/docs/glycerine_-_an_overview.pdf. [Online, accessed: 14 April 2014].

[14] Y. Li, J.e. Zhou, S. Tung, E. Schneider, S. Xi, A review on development of nanofluid preparation and characterization, Powder Technology, 196(2) (2009) 89-101.

[15] U.R. Nanomaterials, Nanopowder: Single-Element Oxides (Al2O3 alpha, 99+%, 80 nm), US Research Nanomaterials, 2014. Available: http://www.us-nano.com/nanopowders. [Online, accessed: 14 April 2014].

[16] MKNano, Nanoparticles: Single-Element-Oxides/Aluminum Oxide Nanopowder (Al2O3-Alpha, 40 nm, 99.5% Pure & Al2O3-Alpha, 100 nm, 99.9% Pure), MKNano, 2014. Available: http://mknano.com/Nanoparticles/Single-Element-Oxides/. [Online, accessed: 14 April 2014].

[17] S.I. Jeol, JEM-2100F Transmission Electron Microscope, JOEL USA, 2015. Available: http://www.jeolusa.com/PRODUCTS/TransmissionElectronMicroscopes%28TEM%29/200kV/JEM-2100F/tabid/208/Default.aspx. [Online, accessed: 6 March 2015].

[18] D. Devices, KD2 Pro thermal properties analyzer operator's manual version 4, in, Decagon Devices, Inc., Pullman, WA, USA, 2015, pp. 1-67.
[19] R. Saleh, N. Putra, R.E. Wibowo, W.N. Septiadi, S.P. Prakoso, Titanium dioxide nanofluids for heat transfer applications, Experimental Thermal and Fluid Science, 52 (2014) 19-29.
[20] B.H. Salman, H.A. Mohammed, K.M. Munisamy, A.S. Kherbeet, Characteristics of heat transfer and fluid flow in microtube and microchannel using conventional fluids and nanofluids: A review, Renewable and Sustainable Energy Reviews, 28 (2013) 848-880.
[21] U.T. Hielscher, UP200H / UP200S – Ultrasonic Power for the Lab, hielscher ultrasonics gmbh 2014. Available: http://www.hielscher.com/200s_p.htm. [Online, accessed: 14 April 2014].
[22] Lauda, Operating instructions: ECO GOLD Heating and cooling thermostat with control head Gold in: 08/2011a1, Lauda Dr. R. Wobser GM BH & CO.KG, 2011, pp. 1 - 119.
[23] G.F. Hewitt, Heat Exchanger Design Handbook 2008: Physical properties, Begell house, New York, USA, 2008, pp. 5.5.10-71.
[24] F.P. Incropera, D.P. DeWitt, Introduction to Heat Transfer, John Wiley & Sons, New York, USA, 1996, pp. 836-844.
[25] S. Horiba, A guidebook to particle size analysis, in, HORIBA Instruments, Irvine, CA, USA, 2012, pp. 1-32.
[26] N.R. Dhineshbabu, G. Karunakaran, R. Suriyaprabha, P. Manivasakan, V. Rajendran, Electrospun MgO/Nylon 6 Hybrid Nanofibers for Protective Clothing, Nano-Micro Letters, 6(1) (2014) 46-54.
[27] V. Baecker, Workshop: Image processing and analysis with ImageJ and MRI Cell Image Analyzer, Montpellier RIO Imaging, 2010. Available: http://www.mri.cnrs.fr/datas/fichiers/articles/60/183.pdf. [Online, accessed: 5 May 2014].
[28] C. Suryanarayana, M.G. Norton, X-ray Diffraction: A Practical Approach, Plenum Publishing Corporation, New York, USA, 1998, pp. 207-221.
[29] A. Garbout, S. Bouattour, A.B. do Rego, A. Ferraria, A. Kolsi, Synthesis, Raman and X-ray diffraction investigations of rubidium-doped Gd 1.8 Ti 2 O 6.7 pyrochlore oxide via a sol–gel process, Journal of Crystal Growth, 304(2) (2007) 374-382.
[30] C. Oprea, V. Ciupina, G. Prodan, Investigation of nanocrystals using TEM micrographs and electron diffraction technique, Roumania Journal of Physics, 53(1-2) (2008) 223-230.
[31] S.A. Speakman, Estimating Crystallite Size Using XRD, MIT Center for Materials Science and Engineering, 2012. Available: www.eng.uc.edu/~beaucag/Classes/.../MITCrystalSizeAnalysis.pdf. [Online, accessed: 10 March 2014].
[32] R.S. Figliola, D.E. Beasley, Theory and design for mechanical measurements, 5th ed., John Wiley & Sons, USA, 2011, pp. 161-198.
[33] D.G.K. Kleinbaum, Lawrence L.; Nizam, Azhar ; Muller, keith E., Applied Regression Analysis and Other Multivariate Methods, 4e ed., Thomson Higher education Belmont, USA, 2008, pp. 305 - 348.

[34] H.J. Berendsen, A student's guide to data and error analysis, Cambridge University Press, 2011, pp. 84-106.
[35] S. Halelfadl, T. Maré, P. Estellé, Efficiency of carbon nanotubes water based nanofluids as coolants, Experimental Thermal and Fluid Science, 53 (2014) 104-110.
[36] I.M. Mahbubul, S.A. Fadhilah, R. Saidur, K.Y. Leong, M.A. Amalina, Thermophysical properties and heat transfer performance of Al2O3/R-134a nanorefrigerants, International Journal of Heat and Mass Transfer, 57(1) (2013) 100-108.
[37] W. Duangthongsuk, S. Wongwises, Measurement of temperature-dependent thermal conductivity and viscosity of TiO2-water nanofluids, Experimental Thermal and Fluid Science, 33(4) (2009) 706-714.
[38] E. Timofeeva, A. Gavrilov, J. McCloskey, Y. Tolmachev, S. Sprunt, L. Lopatina, J. Selinger, Thermal conductivity and particle agglomeration in alumina nanofluids: Experiment and theory, Physical Review E, 76(6) (2007) 1-16.
[39] R.S. Vajjha, D.K. Das, Experimental determination of thermal conductivity of three nanofluids and development of new correlations, International Journal of Heat and Mass Transfer, 52(21-22) (2009) 4675-4682.
[40] M. Kole, T.K. Dey, Effect of prolonged ultrasonication on the thermal conductivity of ZnO–ethylene glycol nanofluids, Thermochimica Acta, 535 (2012) 58-65.
[41] R.S. Khedkar, S.S. Sonawane, K.L. Wasewar, Influence of CuO nanoparticles in enhancing the thermal conductivity of water and monoethylene glycol based nanofluids, International Communications in Heat and Mass Transfer, 39(5) (2012) 665-669.
[42] Y. Xuan, Heat transfer enhancement of nanofuids, International Journal of Heat and Fluid Flow, 21 (2000) 58-64.
[43] T.-P. Teng, Y.-H. Hung, T.-C. Teng, H.-E. Mo, H.-G. Hsu, The effect of alumina/water nanofluid particle size on thermal conductivity, Applied Thermal Engineering, 30(14–15) (2010) 2213-2218.
[44] K.S. Suganthi, K.S. Rajan, Temperature induced changes in ZnO–water nanofluid: zeta potential, size distribution and viscosity profiles, International Journal of Heat and Mass Transfer, 55(25) (2012) 7969-7980.
[45] S.M.S. Murshed, K.C. Leong, C. Yang, Investigations of thermal conductivity and viscosity of nanofluids, International Journal of Thermal Sciences, 47(5) (2008) 560-568.
[46] M. Kole, T.K. Dey, Thermophysical and pool boiling characteristics of ZnO-ethylene glycol nanofluids, International Journal of Thermal Sciences, 62 (2012) 61-70.
[47] H. Xie, W. Yu, W. Chen, MgO nanofluids: higher thermal conductivity and lower viscosity among ethylene glycol-based nanofluids containing oxide nanoparticles, Journal of Experimental Nanoscience, 5(5) (2010) 463-472.
[48] W. Yu, H. Xie, L. Chen, Y. Li, Enhancement of thermal conductivity of kerosene-based Fe3O4 nanofluids prepared via phase-transfer method, Colloids and Surfaces A: Physicochemical and Engineering Aspects, 355(1–3) (2010) 109-113.

[49] M.-S. Liu, M.C.-C. Lin, C.Y. Tsai, C.-C. Wang, Enhancement of thermal conductivity with Cu for nanofluids using chemical reduction method, International Journal of Heat and Mass Transfer, 49(17–18) (2006) 3028-3033.

[50] K.S. Hong, T.-K. Hong, H.-S. Yang, Thermal conductivity of Fe nanofluids depending on the cluster size of nanoparticles, Applied Physics Letters, 88(3) (2006) 1-3.

[51] M. Sharifpur, T. Ntumba, J.P. Meyer, Parametric analysis of effective thermal conductivity models for nanofluids, in: Proceedings of the ASME 2012 International Mechanical Engineering Congress and Exposition, American Society of Mechanical Engineers, Houston, USA, 2012, pp. 1-11.

[52] J. Buongiorno, D.C. Venerus, N. Prabhat, T. McKrell, J. Townsend, R. Christianson, Y.V. Tolmachev, P. Keblinski, L.-w. Hu, J.L. Alvarado, I.C. Bang, S.W. Bishnoi, M. Bonetti, F. Botz, A. Cecere, Y. Chang, G. Chen, H. Chen, S.J. Chung, M.K. Chyu, S.K. Das, R. Di Paola, Y. Ding, F. Dubois, G. Dzido, J. Eapen, W. Escher, D. Funfschilling, Q. Galand, J. Gao, P.E. Gharagozloo, K.E. Goodson, J.G. Gutierrez, H. Hong, M. Horton, K.S. Hwang, C.S. Iorio, S.P. Jang, A.B. Jarzebski, Y. Jiang, L. Jin, S. Kabelac, A. Kamath, M.A. Kedzierski, L.G. Kieng, C. Kim, J.-H. Kim, S. Kim, S.H. Lee, K.C. Leong, I. Manna, B. Michel, R. Ni, H.E. Patel, J. Philip, D. Poulikakos, C. Reynaud, R. Savino, P.K. Singh, P. Song, T. Sundararajan, E. Timofeeva, T. Tritcak, A.N. Turanov, S. Van Vaerenbergh, D. Wen, S. Witharana, C. Yang, W.-H. Yeh, X.-Z. Zhao, S.-Q. Zhou, A benchmark study on the thermal conductivity of nanofluids, Journal of Applied Physics, 106(9) (2009) 1-14.

[53] M. Shaker, E. Birgersson, A. Mujumdar, Extended Maxwell model for the thermal conductivity of nanofluids that accounts for nonlocal heat transfer, International Journal of Thermal Sciences, 84 (2014) 260-266.

[54] H. Ş. Aybar, M. Sharifpur, M. R. Azizian, M. Mehrabi, and J. P. Meyer, A Review of Thermal Conductivity Models of Nanofluids, Heat Transfer Engineering, 36 (13) (2015) 1085-1110, 2015.

[55] M. Corcione, Empirical correlating equations for predicting the effective thermal conductivity and dynamic viscosity of nanofluids, Energy Conversion and Management, 52(1) (2011) 789-793.

[56] C.H. Li, G.P. Peterson, Experimental investigation of temperature and volume fraction variations on the effective thermal conductivity of nanoparticle suspensions (nanofluids), Journal of Applied Physics, 99(8) (2006) 1-8.

[57] C.H. Chon, K.D. Kihm, S.P. Lee, S.U.S. Choi, Empirical correlation finding the role of temperature and particle size for nanofluid (Al 2O 3) thermal conductivity enhancement, Applied Physics Letters, 87(15) (2005) 1-3.